Rapid Reconstitution Packages (RRPs) implemented by integration of computational fluid dynamics (CFD) and 3D printed microfluidics

Rapid Reconstitution Packages (RRPs) Implemented by Integration of Computational Fluid Dynamics (CFD) and 3D Printed Microfluidics

Albert Chi[1], Sebastian Curi[1,3], Kevin Clayton[1], David Luciano[1], Kameron Klauber[1], Alfredo Alexander-Katz[2], Sebastian D'hers[1,3], Noel M. Elman[1,*]

1. Institute for Soldier Nanotechnologies, Massachusetts Institute of Technology, 500 Technology Square, NE47-525, Cambridge, MA, 02139, USA

2. Department of Materials Science and Engineering, Massachusetts Institute of Technology, 77 Massachusetts Avenue, Cambridge, MA, 02139, USA

3. Department of Mechanical Engineering, Instituto Tecnológico de Buenos Aires (ITBA), Ave. Madero 399, A-1-2, Buenos Aires, Argentina, CP 1106

* Corresponding author: Noel Elman, 500 Technology Square, NE47-525, Cambridge, MA, 02139, USA, nelman@mit.edu

Abstract

Rapid Reconstitution Packages (RRPs) are a portable platform that integrates microfluidics for rapid reconstitution of lyophilized drugs. Rapid reconstitution of lyophilized drugs using standard vials and syringes is an error-prone process. RRPs were designed using Computational Fluid Dynamics (CFD) techniques to optimize fluidic structures for rapid mixing, integrating physical properties of targeted drugs and diluents. Devices were manufactured using Stereo Lithography 3D Printing for micrometer structural precision and rapid prototyping.

Tissue plasminogen activator (tPA) was selected as the initial model drug to test the RRPs as it is unstable in solution. tPA is a thrombolytic drug, stored in lyophilized form, required in emergency settings for which rapid reconstitution is of critical importance.

RRP performance and drug stability were evaluated by High Performance Liquid Chromatography (HPLC) to characterize release kinetics. In addition, Enzyme-linked Immuno Sorbent Assays (ELISAs) were performed to test for drug activity after the RRPs were exposed to various controlled temperature conditions. Experimental results showed that RRPs provided effective reconstitution of tPA strongly correlated with CFD results. Simulation and experimental results show that release kinetics can be adjusted by tuning the device structural dimensions and diluent-drug physical parameters. The design of RRPs can be tailored for a number of applications by taking into account physical parameters of the active pharmaceutical ingredients (APIs), excipients and diluents. RRPs are a portable platform that can be utilized for reconstitution of emergency drugs in time-critical therapies.

1. Introduction

Emergency medications in ambulatory settings are formulated and administered often in time-critical situations, leading to an increase in the probability of errors for therapeutic treatment [1-4]. Reconstituting lyophilized drugs is an operational challenge in demanding environments, e.g. disaster zones, battlefield support, and rural areas. Heat insulation is critical for biological drugs, e.g. antibodies, for which the efficacy of the active pharmaceutical ingredient (API) heavily relies on biomolecular conformality. Small molecule drugs consisting of pure chemical formulation are often deployed in liquid form in hermetically packaged glass ampules. In order to avoid hydrolysis, biological drugs are stored in lyophilized form in hermetically sealed glass vials that require subsequent reconstitution upon delivery. Lyophilization process involves freeze-drying the API combined with excipients, rendering a powder form with specific physical properties that include mass density, solubility, structure (either amorphous, crystalline or combination) and packing factor.

The steps for drug reconstitution in vials require: injecting specific diluents into the vials, manual shaking and visually confirming homogeneity [5]. Various pre-filled dual-chamber solutions exist for on-demand reconstitution. These solutions typically rely on solubility between a diluent and lyophilized drug and still require manual shaking. The design of these devices typically consists of two chambers: one for the drug in lyophilized form (solute) and another for the diluent (solvent). Dual-chamber devices have been utilized for small API payloads with a limited number of pharmacological therapies, such as human growth hormone (HGH) commercially known as Genotropin (Pfizer, Inc.) [6].

In order to effectively reconstitute lyophilized drugs with large payloads (e.g. antibiotics and biological drugs in the order of tens of milligrams) and low solubility APIs, numerical

models should be considered. The challenge lies on the design of devices to perform optimal reconstitution incorporating parameterization models of APIs, excipients and diluents, while designing microfluidic structures to optimize mixing homogeneity and response time as a function of input shear flows [7]. The next generation of reconstitution devices for large payloads (10 mg – 250 mg) and low solubility APIs will therefore require a comprehensive design consolidation of physical parameters to optimize mixing.

Rapid Reconstitution Packages (RRPs) were designed with numerical methods integrating microfluidic structures to dramatically enhance mixing of large payloads to optimize mixing in the 1-7 sec range. RRPs were designed using Computational Fluid Dynamics (CFD) models that incorporate parameterization of physical properties of lyophilized drugs and diluents. CFD modeling provided insights into the flow distribution variables of drug dissolution, such as turbulence, solubility, vorticity and shear stress. Figure 1 shows a schematic diagram of the RRP describing the different components and critical dimensions.

Device performance was evaluated by selecting Tissue Plasminogen Activator (tPA) as the initial model drug. tPA is a commonly used thrombolytic for treating ischemic stroke and myocardial infarction (MI) [8,9]. tPA is a large peptide-based molecule, reportedly unstable in liquid form (up to 8 hours in solution) [10]**.** The drug was selected for investigation as it is normally administered in emergency situations. The tPA used for experiments was Cathflo Activase recombinant (Genentech, Inc.). Emergency protocols for acute ischemic stroke require approximately a dose of 40-90 mg intravenous injection and 4-9 mg bolus injection according patient's weight [11].

RRPs were designed from a clinical perspective to improve logistics for emergency and ambulatory applications in a single-step process. RRPs promise a novel delivery modality of

APIs, which are unstable in liquid form, in wide variety of applications for emergency and ambulatory settings.

2. Materials and Methods

2.1 Device Design

The RRP design was initially conceived as a cylindrical cartridge that can be activated by inserting into a standard syringe and compressed with the syringe plunger. This mode of operation was selected to help preserve the standard operating procedure of drug delivery using syringes. RRPs are designed to fit in 10, 20 and 50 mL syringes, depending on the target pharmacological therapy that corresponds to payload volume. RRPs were designed for operation in three steps. First, the syringe plunger is removed from the syringe barrel. Second, the RRP is placed inside of the syringe barrel as a cartridge. Finally, the syringe plunger is reinserted into the syringe barrel and put into firm contact with the RRP. The system is then ready for operation. Figure 2 shows a fabricated RRP placed inside of a standard 20 mL syringe. The device relies on the telescopic operation of an internal plunger which opens a valve between the diluent chamber and drug chamber, forcing the diluent into the drug chamber. The drug-diluent product is then further mixed in the mixing chamber and then ejected. The fluid flow path is shown in Figure 3. A safety mechanism will be incorporated in the future to prevent accidental activation, e.g. requiring a twisting motion prior to use.

2.3 Numerical Modeling and Physical Considerations

Computational Fluid Dynamics (CFD) techniques were employed to quantitatively optimize RRP reconstitution performance. Figure 4 shows a flow diagram illustrating how design, CFD, and experiments were all influenced and informed by each process. The use of

CFD provides a set of powerful quantitative techniques for gaining insights into the design of structures intended to optimize mixing parameters for drug mixing, advection, and diffusion phenomena [12-17]. The numerical simulations were performed using a CFD modeling platform (Flow-3D, Flow Science, Inc.), that uses a Finite Volume Method combined with a Volume of Fluid Method for free surface tracking [18,19]. For modeling turbulence, a κ-ε model with Re-Normalization Group (RNG) was adopted. This approach allowed the observation of different dimensional scales present in the simulation, providing predictions for mass transfer [20,21]. Additionally, a second order projection method was used for solving Navier-Stokes equations in transient analysis with a second order scalar transport model.

Considering device symmetry, simulations were run on a $1/12^{th}$ cylindrical domain, at the expense of neglecting angular flow to limit computational load. The mesh adopted for simulations included approximately 10^6 finite volumes. Figure 5 shows a schematic diagram of the RRP with detailed meshed structure. Boundary conditions were defined as fixed velocity at input, no slip at the walls and fixed pressure at the output. The resulting average time step for optimized convergence was approximately 30 μs.

Preliminary analyses only focused on diluent flow across structures. The primary objectives for these simulations were defined as follows: (1) Increase inlet velocity into the drug chamber, (2) minimize stagnation-prone regions, and (3) streamline the fluid flow while increasing advection. Inlet velocity information could be utilized to increase turbulence and vorticity in the drug chamber for improving mixing. Stagnation-prone regions were to be avoided to maximize drug exhaustion. Streamlining was crucial for the overall design optimization.

A more comprehensive CFD model with diluent-drug interactions was introduced to simulate the drug reconstitution process in the preliminarily simulated designs. Physical parameters of the drug and excipients were incorporated into the model.

Cathflo Activase in its delivered form was composed of a 1:40 API to excipient, with 2 mg tPA and 78 mg excipients (sucrose, L-arginine, polysorbate 80, and phosphoric acid), summing up to 80 mg per payload. The entire payload was modeled as a homogeneous compound of sucrose (the major component in the lyophilized composition) with a diffusivity value in water equal to 5x10E-8 m^2/s, a crystalline mass density of 1.587 mg/mm^3 and an amorphous mass density of 1.507 mg/mm^3. A homogenous mixture of tPA and excipient was assumed in order to quantify API output concentration as $1/40^{th}$ of the total output scalar concentration obtained from simulations.

The packing factor due to lyophilization was taken into account to incorporate the stacking of the drug into a singular annular volume defined in the drug chamber. The packing factor was estimated as follows [22]:

$$PF = \frac{NV_{sphere}}{V_{drug}} = \pi \quad \frac{}{18} \approx 0.74 \tag{1}$$

Where N is the number of particles, V_{sphere} is the particle volume approximated as sphere of diameter, d, and V_{drug} is the volume of the drug, distributed as a ring in the drug chamber. The density of the lyophilized drug excipient mixture, taking into account the packing factor, was estimated at 1.2 mg/mm^3.

Distilled ultrapure water was selected as the model diluent. The modeled water was assumed to be Newtonian and incompressible. Gravity and surface tension effects were neglected for the Newtonian fluid as the Froude number, defined as the ratio of inertia to gravity

forces, and Weber number, defined as ratio of inertia to surface tension forces, were both much greater than unity.

The effect of flow on drug dissolution upon initial device activation was introduced as a change in effective viscosity, estimated by approximating the resulting solution as a dilute suspension of small rigid spherical particles, estimated as follows [23]:

$$\mu_{eff} = \mu_f \frac{1}{(1-\varphi)^{2.5}} \cong \mu_f(1 + 2.5\varphi) \quad (2)$$

Where μ_{eff} is the effective viscosity of the diluent, μ_f is the viscosity of the fluid without solute and φ is the volume fraction, defined as the diluent volume to the mixed volume.

To assess the device behavior under possible operation conditions, numerical simulations were carried out for three different locations of the drug (tPA) within the drug chamber and four distinct activation times of the RRP defined as follows: 1 s, 2 s, 4 s and 7 s. The activation time is the time needed give a shot, which were chosen to emulate real operation times of syringes. The location of drug was modeled at different positions to investigate effect in the output release kinetics. The three different simulated positions of drugs are shown in Figure 6 as cross sectional areas of a ring. Position 1 represents the location of the drug RRP on top of the chamber. Position 2 represents the middle position of the drug with the highest probability of being located without any external force acting on it. Position 3 represents the location of the drug RRP on the bottom of the chamber. The activation time was defined from the time of valve opening to the full compression of the internal plunger. A data probe to measure concentration gradients as function of time was defined at the outlet of the RRPs in the simulations.

2.3 RRP Fabrication

Each part of the RRP was designed using CAD (SolidWorks 2013, Solidworks, Inc.). CAD files were loaded into a 3D printing platform manager called 3D Manage (3D Systems, Inc.). RRP parts were fabricated through Stereo Lithographic 3D printing (Projet 6000, 3D Systems, Inc.). 3D structures were formed layer-by-layer on an actuated plate that moved into a resin bath. The printer resolution at the highest definition settings was defined as 50 μm in the z-axis (each vertical layer), 10 μm in lateral dimensions. The resin was a liquid, light-polymerizable acrylic plastic (VisiJet® Clear, 3D Systems, Inc.). The material properties were as follows: mass density was 1.1 g/cm^3 at 25°C, tensile modulus was 2560 MPa, flexural modulus was 2330 MPa, glass transition temperature was 70 °C. After printing was completed, each part was cleaned in an isopropanol bath for 30 min., in water bath for 30 min., and subsequently cured in an UV oven for 30 min. The resulting parts were then assembled into fully functional RRPs.

2.4 Sample Preparation

RRPs were initially kept at 20 ºC, and subsequently subjected to a fixed wall temperature of 65 ºC for 3 hours. Six sample preparations were defined as follows: (1) Standard Cathflo Activase lyophilized in glass vial at 20 ˚C; (2) Cathflo Activase reconstituted in Millipore filtered water and kept in glass vial at 20 ˚C; (3) lyophilized Cathflo Activase loaded into RRPs and kept at 20 ˚C; (4) Cathflo Activase lyophilized in glass vial at 65 ˚C; (5) Cathflo Activase reconstituted in Millipore filtered water and stored in glass vial at 65 ˚C, and (6) Cathflo Activase loaded into RRP and kept at 65 ˚C. Samples were heated inside a silica-desiccated beaker that was placed inside a silicone-oil heat bath for 24 hours prior to assay preparation.

After 24 hours each sample in lyophilized form, including those stored in the RRP, was reconstituted in 2 mL Millipore water, and apportioned for subsequent use in ELISA, UV-vis and HPLC assays.

2.5 Flow Output Characterization

RRPs were loaded with Cathflo Activase (2 mg of tPA and 78 mg of excipients). Each RRP was placed in a 25 cc syringe (Exel International, Co.). Each syringe was then fixed into a syringe pump (Customized 4X PhD Series, Harvard Apparatus, Inc.) that activated the RRP at a rate of choice. The syringe pump was set to inject a standard 20 cc volume syringe at a flow rate of 260 mL/min for a total inject time of two seconds. As the flow began to emerge from the outlet of the syringe, a customized linear actuator collected the elution. This linear actuator was configured with a collection tray consisting of 14 wells with a fixed width, such that each well represented a time increment of approximately 140 ms. An illustration of the experimental setup is shown in Figure 7. The concentrations of drug in each well were analyzed using a UV spectrometer (Model: 8453 UV-Vis, Spectroscopy System, Agilent Technologies, Inc.) at 210 and 280 nm wavelength with a 100 µL microcuvette (Model 701M10.100B, NGS Precision, Inc.). Concentration for each individual flow increment was measured for multiple trials. The data for all trials was then compiled and compared against a calibration curve, and the average concentration profile of tPA in the eject was derived.

2.6 Activity Assays

Immunoassays were performed to characterize the RRP with standard vials at various conditions to analyze and compare the performance of RRPs. Enzyme-Linked Immunosorbent

Assays (ELISAs) were chosen to analyze activity of tPA after storage. ELISAs enabled the capture and detection of active protein, i.e. tPA, to assess the general stability of drug after storage and reconstitution. A period of 24 hours was chosen since tPA was deemed unstable by the manufacturer in aqueous solution over 8 hours at room temperature (20 °C). HPLC assays were not sufficient in assaying stability for tPA as the low pH buffer required denatured tPA regardless of conformation or partial denaturation already induced by temperature conditions during stress tests of samples. ELISA assays were used to test for stability of samples (Human tPA Platinum ELISA Kit, eBioscience, Inc.) that were exposed to two temperature conditions for approximately 24 hours, T = 20, 65 ˚C. The samples to be tested were injected into each ELISA well and left to incubate. After a wash step, a second antibody, horseradish peroxidase (HRP)-conjugated anti-tPA, was injected into each sample well. The HRP-conjugated anti-tPA bound onto the opposing side of the tPA molecule already bound onto the plate-fixed antibody. After a second wash step, a color inducing substrate (TMB substrate) was then injected into the wells, which bound onto the HRP to induce a measureable gradient representing the amount of tPA bound. In order to prevent oversaturation of the antibodies, the samples were diluted to 10 ng/mL to fall within the assay sensitivity range of 2 pg/mL - 10 ng/mL. Optical signal intensity from assay plates were measured with spectrophotometer at wavelength 450 nm (PowerWave HT Microplate Spectrophotomer, BioTek Instruments, Inc.). Each sample was normalized against a calibration curve derived from a 5-parameter logistic fit of tPA standards ran concurrently with the samples.

2.7 Total Output Concentration Analysis

High Performance Liquid Chromatography (HPLC) was carried out to analyze and compare the total concentration of output delivered by each tested drug delivery modality (standard vials and RRPs). This analysis was performed to determine and compare the concentration of reconstituted product through the RRP and standard mixing in vial. Each sample was initially loaded with 1:1 diluent:drug prior to mixing. HPLC (1100 Model, Agilent Technologies, Inc.) was performed with each sample referenced against a calibration curve for the drug being measured. Assays were performed with a reversed-phase column (ZORBAX SB-CN, 4.6 mm x 250 mm column with 5 µL pores, Agilent Technologies, Inc.). The mobile phase was a gradient with an initial hold for 5 min in a ratio of 70:30:0.1 water:acetonitrile (ACN):trifluoroacetic acid (TFA), brought to 50:50:0.1 water:ACN:TFA over 80 min, and subsequently to 100:0.1 ACN:TFA over 15 min. An acidic environment (created by the use of TFA, pKa = 0.23) was necessary to separate tPA from solution. Flow rate was 1 mL/min and injection volume was 250 µL. tPA presence was detected by UV spectrometry at 280 nm.

3. Results

3.1 Simulation Results: Velocity and Vorticity

Simulation results with flow characterization models allowed for incremental, yet significant design changes to improve efficiency of drug mixing. Figure 8 shows three design generations and corresponding snapshots during simulated activation times. Velocity magnitudes are represented in these figures to provide quantification of concentration values in the device. Figures 8A-C show the jet effect across the drug chamber. Initial design optimization focused on increasing jet velocity, whereas later designs focused on deflecting the direction the jet

downwards for greater mixing in the drug chamber. The change in jet direction corresponded with design changes in the drug chamber, aimed at further increasing mixing while eliminating stagnation regions.

To perform parametric design comparison, average vorticity was defined by calculating a cell volume weighted average of the absolute value of vorticity of the fluid for every single fluid cell of the meshed structure. A visual representation of average vorticity across fluid cells is shown in Figure 9A. This global estimator provided the mixing performance of the device over the operational time, as shown in Figure 9B, where the impact of design optimization can be demonstrated.

A design requirement that became apparent from observing flow streamlines through the RRP was the addition of a compartmentalized mechanism that would prevent drug powder from exiting the drug chamber too soon. Implementation of such a solution was achieved by adding a secondary valve in order to close the chamber exhaust area during the initial transient mixing. Figure 10 shows the steady state flow pattern where streamlines can be identified.

3.2 Simulation Results: Overall Performance

Simulation results initially showed that a jet of solvent entering the drug chamber collided with the drug particles as the RRP was activated. This step proved to be a complex process to model due to the combination of drag forces, dissolution and forced convection. Convection was considered the dominant mass transport mechanism for modeling dissolution. The resulting mixed solution was modeled using constant density ratios of API over excipients calculated from Eq. (1) and effective viscosity from Eq. (2). The drug mixing models showed that most of the reconstitution occurred in the drug chamber. The inlet jet effect caused by the

opening of the valve between the drug chamber and the diluent reservoir increased reconstitution performance. The fraction of drug that does not exit the chamber dragged by the initial flow ends up in localized stagnation regions and slowly diffuses through advection towards the exhaust.

The flow pattern belonging to drug in position 1 is shown in Figure 11A, showing concentration as a function of time as snapshots of the simulations runs. Total results from simulations quantifying concentration eluted from RRPs as a function of time for various locations and injection times are summarized in Figure 11B. The simulated curves resembled Weibull or log-normal distributions, with a larger distribution of drug output towards the onset of activation followed by a tail. These results were in accordance with subsequent experimental observations, showing that most of the mixing occurred during the initial activation of the RRP with a tail of drug convection. A double peak was observed for the 1 s activation time most likely due to complex flows in the drug chamber caused by the higher velocities. Single peaks were observed for longer activation times ($t \geq 2$ s). The output concentration profiles varied significantly with the activation times, indicating that the release kinetics could be significantly tailored by adjusting the input flow rate. The concentration distribution for different drug location runs was more uniform for longer activation times. This effect was attributed to diffusion having a greater impact on drug dissolution as flow rate decreases.

Figure 11C shows the total amount of drug that was eluted from the RRP after full activation. The total output amount from the RRP was not significantly changed by payload size, initial drug location, or rate of injection, indicating that flow rate may indeed have an effect in concentration profiles but not in the total mass of drug delivered. Simulations for various amounts of tPA were carried out with 1, 4, 10, 30, 60, and 100 mg payloads, which resulted in similar total normalized outputs, as shown in Figure 12.

3.3 Experimental Results

Figure 13 shows results of ELISA trials of the defined six tPA samples stored in different temperature conditions (T = 20, 65 ˚C) for N = 6. ELISAs showed tPA preservation of activity over 24 hours for all samples (solid, liquid, and RRP) at 20 ˚C. Interestingly, tPA in liquid form was able to maintain its activity beyond its cited 8 hour limit. tPA stored in reconstituted form within glass vials at 65 ˚C suffered the greatest loss of activity, expressing only 39.3 % in average of the standard activity average. RRPs proved slightly better at retaining drug stability at the critically high temperature of 65 ˚C than lyophilized drug stored in a standard glass vial with a significant difference, retaining 86.3 % in average of total initial drug stability average as opposed to 81.6 % average activity in the glass vial.

In order to characterize the concentration profile from the RRPs, a 2 s injection time was chosen to emulate a typical injection time as delivered by a clinician. The concentration output of all samples analyzed by HPLC (N = 8) did not show a significant difference in variability, as shown in Figure 14.

4. Discussion

The RRP design was optimized by numerical models using CFD models ultimately to maximize reconstitution. The numerical models allow simulations of reconstitution performance for specific pharmacological formulation with different injection times and payloads. Experimental results showed the reliability of simulated results, within the same order of magnitude, in concentration outputs as a function of response time. Results from the experimental studies compared to the modeled results are shown in Figure 15. Experiments revealed that drug became allocated mostly on the sidewalls and bottom of the drug chamber.

Consequently, Position 3 was adopted for the simulation as the most representative drug position within the drug chamber, and subsequently incorporated into the numerical model for correlation analysis with the experimental results.

Experimental variability can be mainly attributed to errors in the discrete sample collection method, primarily related to differences in volume amounts in microliter range per sample. Another source of variability can be attributed to the slightly different locations of lyophilized APIs between different generations of RRPs, as the drug powder cannot be localized precisely within the drug chamber. This method is not sensitive to quickly changing concentration profiles. A continuous measurement method will be implemented in future work to characterize release kinetics with higher precision. The numerical model described the dominant physical phenomena fairly well and to provide tools for design. The mechanism of mixture-wall adhesion and the behavior of low solubility mixtures must be addressed in order to be able to model the wide range of pharmacological formulation available.

Each pharmacological formulation requires a set of customized parameters that take into account the physical properties of the API, excipients, and diluents. Experimentally determined concentration profiles are critical for performance and safety. For example, the value of the concentration peak can serve as a limiting factor in the design and optimization of the RRP so it does not reach a specific concentration of toxicity. Conversely, the models can be parameterized to the desired delivery profile in order to inform the design of the fluidic structures. For example, the relative position of the payload within the drug chamber can be considered a design parameter to adjust according to the targeted release kinetics. Simulation results have shown that the Position 3 under activation time of 1 s can be regarded as a bolus application for a drug,

whereas Position 1 and activation time of 4 s can be useful for a more continuous release of the same drug.

The payload released has a critical impact in controlling the total dosage delivered in a given pharmacological application. It must be emphasized that the proposed reconstitution model assumes that drug dissolves instantaneously, hence not taking into account drag effects that are experienced by a small portion of solid particles. A more comprehensive model would be required to describe particles that are reconstituted while they are transported.

The presented model allows for simulations results to be incorporated back into the design process, which in turn are quickly implemented using a 3D printing technology. The integrated use of 3D printing technology for the construction of simulated structures provided an advanced approach for accelerating prototyping of microstructures. The computational-experimental iterations provide a method for validating and optimizing reconstitution performance based on structural dimensions and physical parameters. Overall, simulations provide a predictive analytical method, rendering engineering optimization of the RRPs.

Experimental methods including ELISA, HPLC, and flow characterization provided quantitative results required to inform design decisions and ensure design robustness. The integration of CFD models for design of RRPs could be extended to other lyophilized drugs that are required for emergency applications.

RRP integrates microstructures to optimize reconstitution. High solubility, low payload (microgram range) pharmaceutical drugs would not necessarily require such an optimization. The key advantage of the RRP, however, is that it is designed to optimize reconstitution for high solubility, high payload (milligram range) drugs. In the future, implantable controlled drug

delivery systems based on Micro-Electro-Mechanical-Systems (MEMS) will make use of the same microfluidic principles to optimize reconstitution and provide in vivo delivery [24].

5. Conclusions

Rapid Reconstitution Packages (RRPs) were designed using Computational Fluid Dynamics (CFD) models. Predictive models provided an analytical methodology to investigate microfluidic structures that integrate a multitude of physical properties of targeted drugs and diluents. Rapid prototyping of designs using Stereo Lithographic Apparatus (SLA) provides a method to accelerate iteration cycles between computational modeling, design changes and physical validation. Tissue plasminogen activator (tPA), a commonly used thrombolytic for stroke patients, was used as the initial model drug to test the RRPs. CFD results showed closely related behavior to experimental results revealing that RRPs provided effective storage and reconstitution of tPA. We were able to capture the drug concentrations well enough to inform design decisions. The mean concentration was captured precisely, however the instantaneous concentration over the course of device activation can be improved. CFD and experimental results show that release kinetics can be adjusted by modifying device design and diluent-drug physical parameters. The design of RRPs can be tailored for a number of applications by taking into account physical parameters of the active pharmaceutical ingredient (API), excipients and diluents. RRPs represent a portable platform that can be utilized for reconstitution of emergency drugs in time-critical therapies.

6. Acknowledgements

This research work was supported by the US Army Research Office via the Institute for Soldier Nanotechnologies (ISN) at MIT (contract: W911NF-07-D-0004). Albert Chi, Sebastian Curi, Kevin Clayton, David Luciano, Kameron Klauber, Alfredo Alexander-Katz, Sebastian D'hers and Noel M. Elman declare no conflict of interest related to this manuscript.

7. References

1. Parshuram CS, T.T., Seto W, Trope A, Koren G, Laupacis A, *Systematic evaluation of errors occurring during the preparation of intravenous medication.* CMAJ, 2008. **178**(1): p. 42-48

2. McDowell SE, M.-I.S., Ashby D, Ferner RE, *Where errors occur in the preparation and administration of intravenous medicines: a systematic review and Bayesian analysis.* Qual Saf Health Care, 2010. **19**: p. 341-345.

3. JK, A., *Medication errors: what they are, how they happen, and how to avoid them.* Q J Med, 2009. **102**: p. 513-521.

4. Wheeler DW, D.B., Sehmi JS, Burnstein RW, Menon DK, Gupta AK, *Variability in the concentrations of intravenous drug infusions prepared in a critical care unit.* Intensive Care Medicine, 2008. **34**(8): p. 1441-1447.

5. Abeysekera A, B.I., Kluger MT, Short TG, *Drug error in anaesthetic practice: a review of 896 reports from the Australian Incident Monitoring Study database.* Anaesthesia, 2005. **60**(3).

6. Pfizer, I., *Genotropin: somatropin [rDNA origin] for injection (package insert)*, Revised August 2006: New York, NY.

7. Grassby PF, H.L., *Factors affecting the physical and chemical stability of morphine solutions stored in syringes.* International Journal of Pharmacy Practice, 1993. **2**(1): p. 39-43.

8. Hacke W, K.M., Fieschi C, von Kummer R, Davalos A, Meier D, Larrue V, Bluhmki E, Davis S, Donnan G, Schneider D, Diez-Tejedor E, Trouillas P, *Randomised double-blind placebo-controlled trial of thrombolytic therapy with intravenous alteplase in acute ischaemic stroke (ECASS II). Second European-Australasian Acute Stroke Study Investigators.* Lancet, 1998. **352**(9136): p. 1245-1251.

9. The GUSTO investigators, *An international randomized trial comparing four thrombolytic strategies for acute myocardial infarction.* New England Journal of Medicine, 1993. **329**(10): p. 673-682.

10. Genentech, I., *Alteplase (package insert)*, 2005: South San Francisco, CA.

11. t-PA Dosing Chart (estimagedd weight). Storke and Cerebrovascular Center. Boston Medical Center. 2014. http://www.bmc.org/stroke-cerebrovascular/services/acute-stroke-protocol-tPA-dosing-chart.htm

12. Garcia E, K.J., Hatch AV, Hawkins KR, Yager P, *Controlled Microfluidic Reconstitution of Functional Protein from an Anhydrous Storage Depot.* Lab on a Chip, 2004. **4**(1): p. 78-82.

13. Bendek A, L.J., *Automatic Reconstitution Injector Device,* U.S.P.a.T. Office, Editor 2012.

14. May-Newman K, M.M., Lee MN, *Design and Preliminary Testing of a Novel Dual-Chambered Syringe.* Journal of Medical Devices, 2011. **5**(2): p. 037001-1.

15. Kremer DM, H.B., *Process simulation in the pharmaceutical industry: a review of some basic physical models.* Jouranl of Pharmaceutical Sciences, 2006. **95**(3): p. 517-529.

16. Cortes-Quiroza CA, A.A., Zangeneha M, Gotob A, *Analysis and multi-criteria design optimization of geometric characteristics of grooved micromixer.* Chemical Engineering Journal, 2010. **160**(3): p. 852-864.

17. Broboana D, M.B.C., Wohland T, Balan C, *Investigations of the unsteady diffusion process in microchannels.* Chemical Engineering Science, 2011. **66**: p. 1962-1972.

18. CW, H. *Volume-Fraction Techniques: Powerful Tools for Flow Modeling*. in *Computational Wind Engineering Conference*. 1992. University of Tokyo: Flow Science.

19. Isfahani AHG, B.J., *On the Implementation of Two-equation Turbulence Models in FLOW-3D®,* 2009, Flow Sciences, Inc.

20. Yakhot V, O.S., *Renormalization Group Analysis of Turbulence. I. Basic Theory.* Journal of Scientific Computing, 1986. **1**(1): p. 3-51.

21. Nagano Y, I.Y., *Renormalization group theory for turbulence: Assessment of the Yakhot-Orszag-Smith theory.* Fluid Dynamics Research, 1997. **20**(1-6): p. 152-172.

22. Theodore, L., *NanoTechnology: Basic Calculations for Engineers and Scientists*2006, New York: John Wiley & Sons, Inc.

23. Xuan Y, R.W., *Conceptions for heat transfer correlation of nanofluids.* International Journal of Mass Transfer, 2000. **43**: p. 3701-3707.

24. Elman N, Patta Y, Scott A, Masi B, Ho Duc H, Cima M. "The Next Generation of Drug-Delivery Microdevices" Clinical Pharmacology and Theraputics, 1009. **85**(5): p. 544-547. 2009.

7. Figures

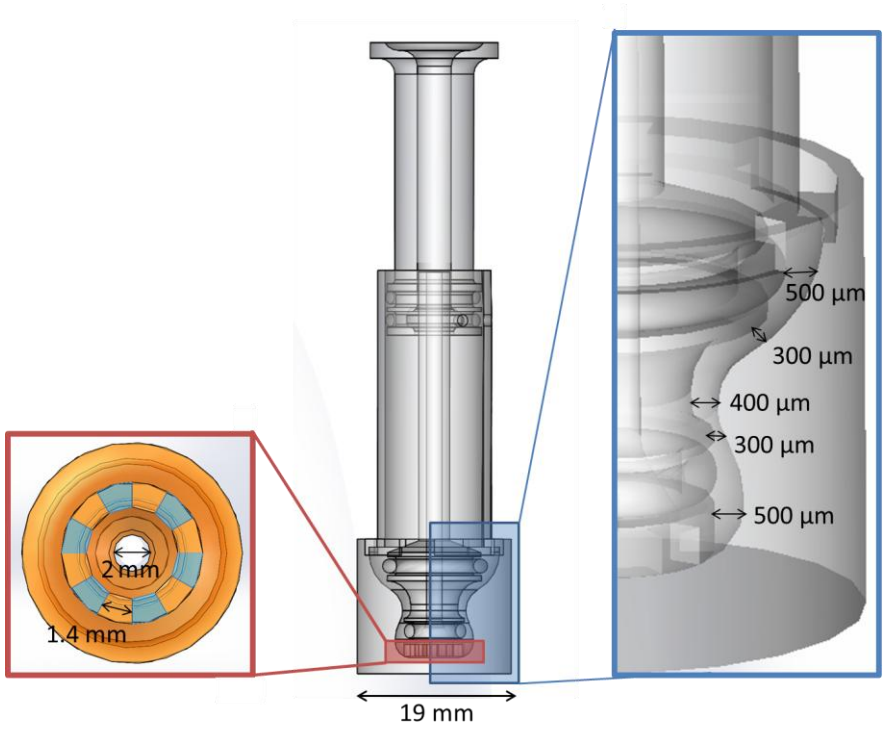

Figure 1: Rapid Reconstitution Package. A. Schematic diagram of RRP. Inset is a zoomed in perspective of the drug and mixing chambers.

Figure 2: Fully assembled RRP device printed by 3D printer.

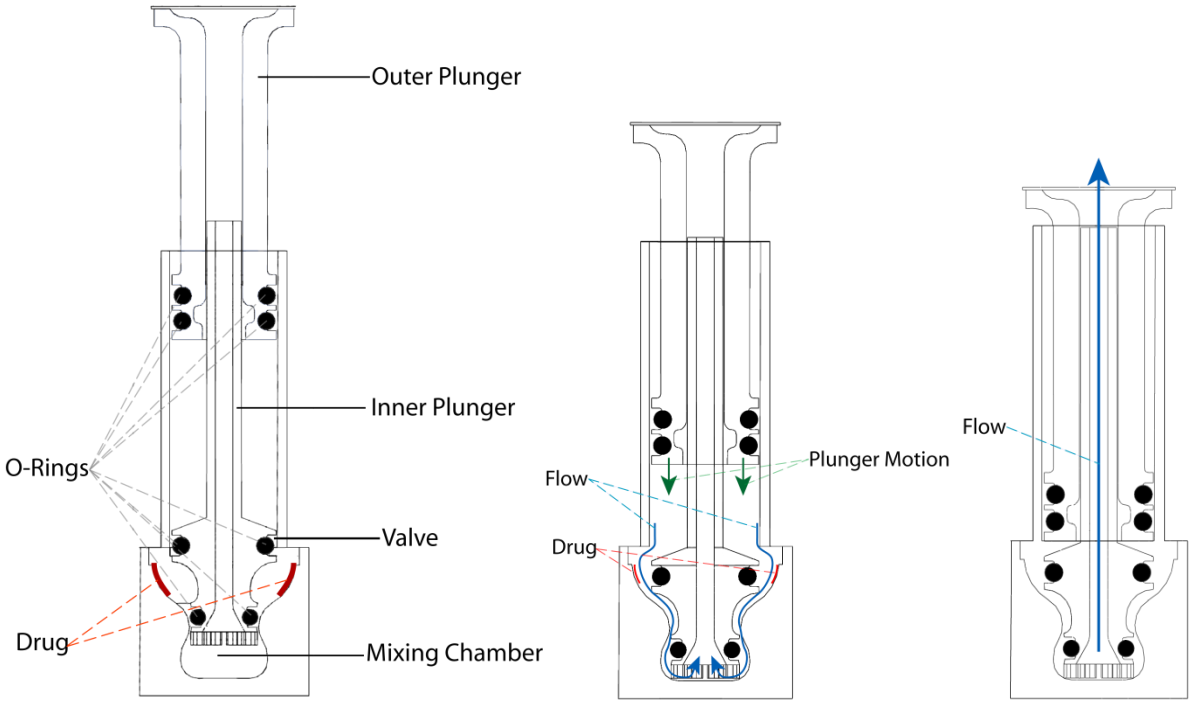

Figure 3: Basic schematic process and activation steps for RRP. The telescopic design of the RRP allows the syringe plunger to press forward collapsing the RRP forcing mixing and outflow of the reconstituted drug. RRP parts, drug placement (red), and flow direction (blue) are labeled.

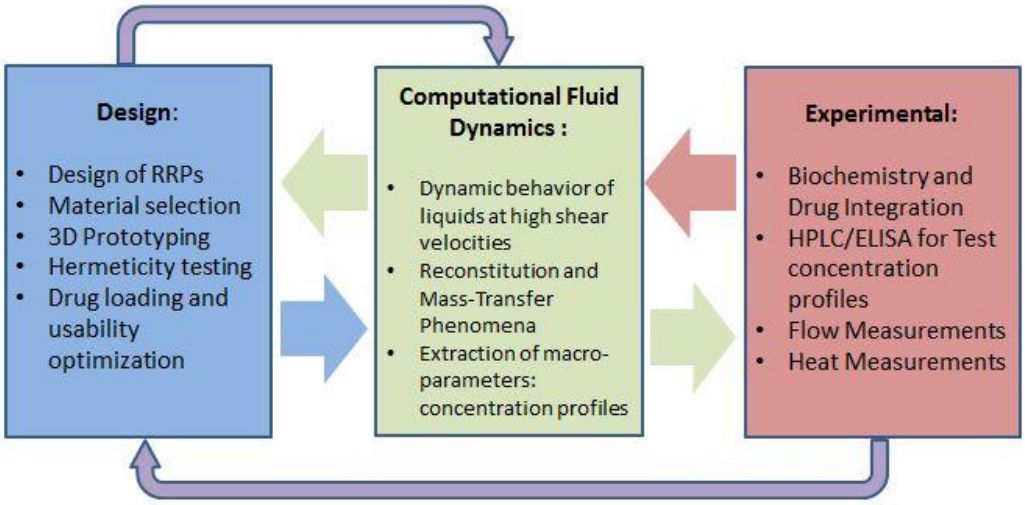

Figure 4: The iterative design process of the RRP is a constant feedback system. Design includes the prototyping and testing of physical properties of the device. Computational fluid dynamics incorporates modeling and numerical processing of results of experiments and tests. Experimental data provides the basis for model optimization, design modification, as well as characterization of the drug reconstitution and device.

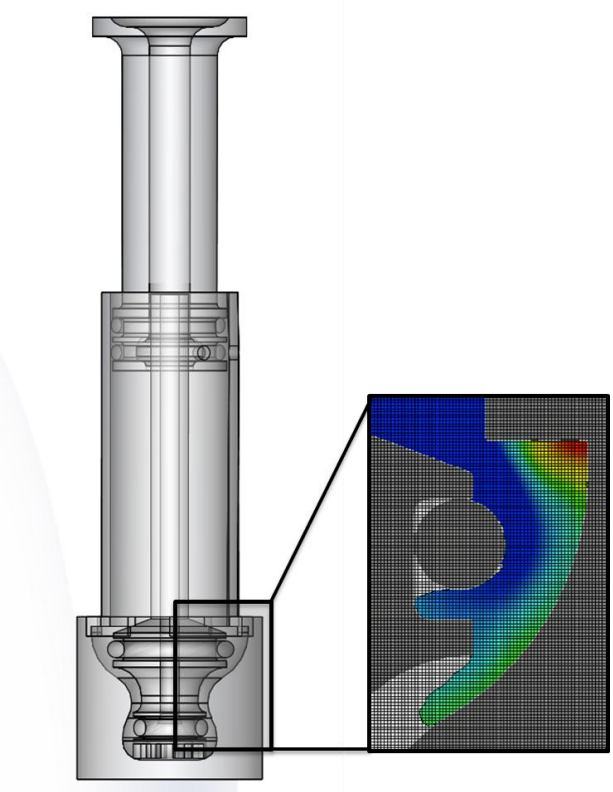

Figure 5: The axial profile of the RRP is used to simplify computation. 1/12th of the structure is simulated. A representation of the mesh-field used to discretize, or divide, the RRP at very fine elements (1 million voxels) for regional calculation is shown.

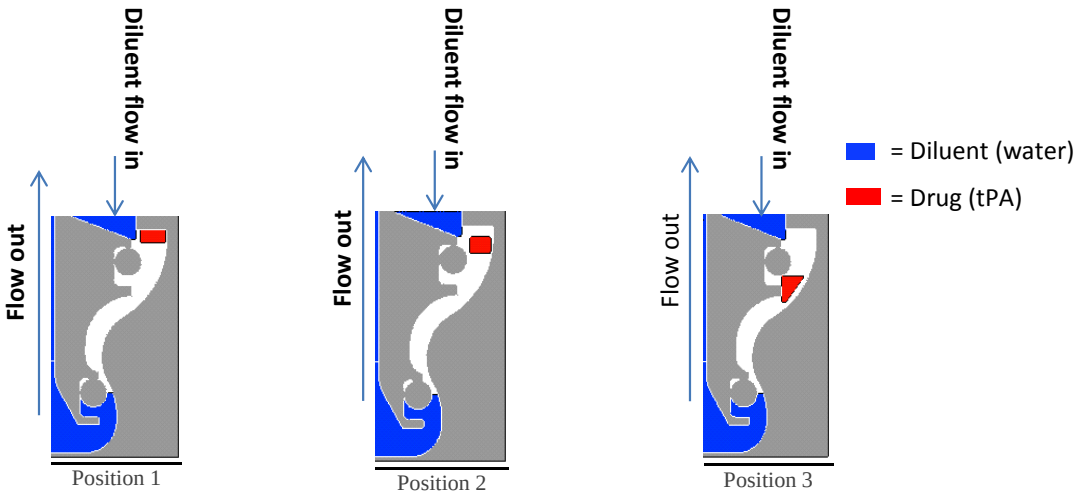

Figure 6: By varying the drug locations in the mixing chamber of the RRP different drug concentration profiles could be obtained from the output of the RRP. The shape here represents ½ of the bottom-half of the device. Position 1 is the top-most position of the drug chamber nearest to the diluent chamber. Position 2 is in the middle of the drug chamber. Position 3 is located towards the bottom of the drug chamber nearest the mixing chamber. Flow direction and diluent chamber orientation are noted on the figures.

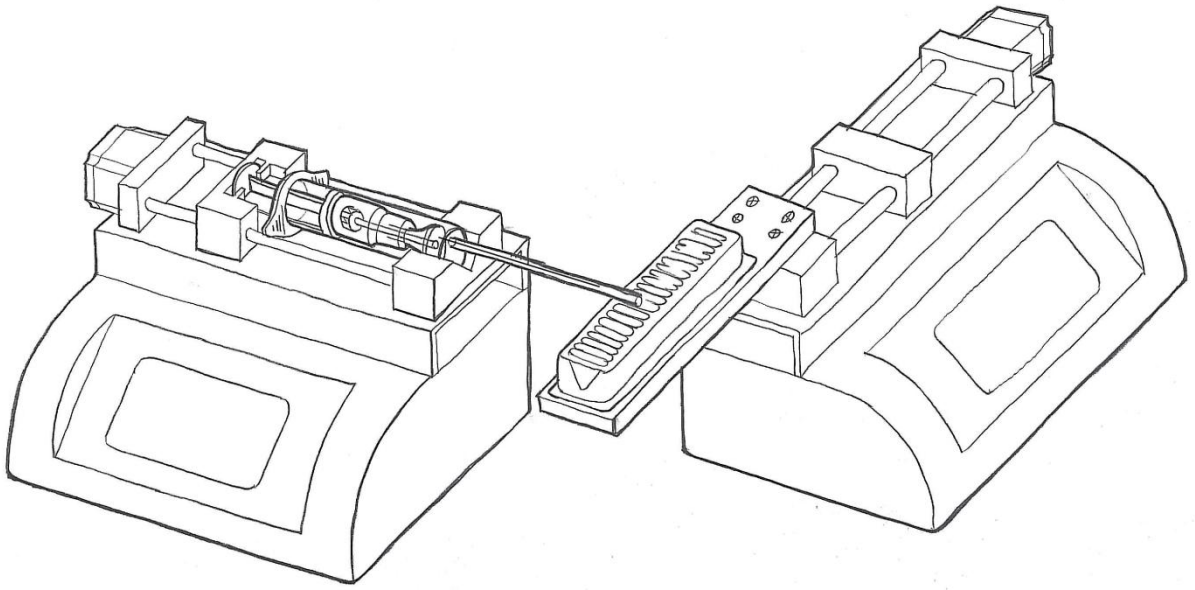

Figure 7: The output collection system used to experimentally characterize flow output of the RRP. A syringe-pump was synchronized with a linear actuator that moves a collection tray. The collection tray had a series of wells representing periods of 0.14 s over a 2 s total injection time. Each well's content was measured for drug concentration using UV-spectroscopy (wavelengths at 210 nm and 280 nm).

A.

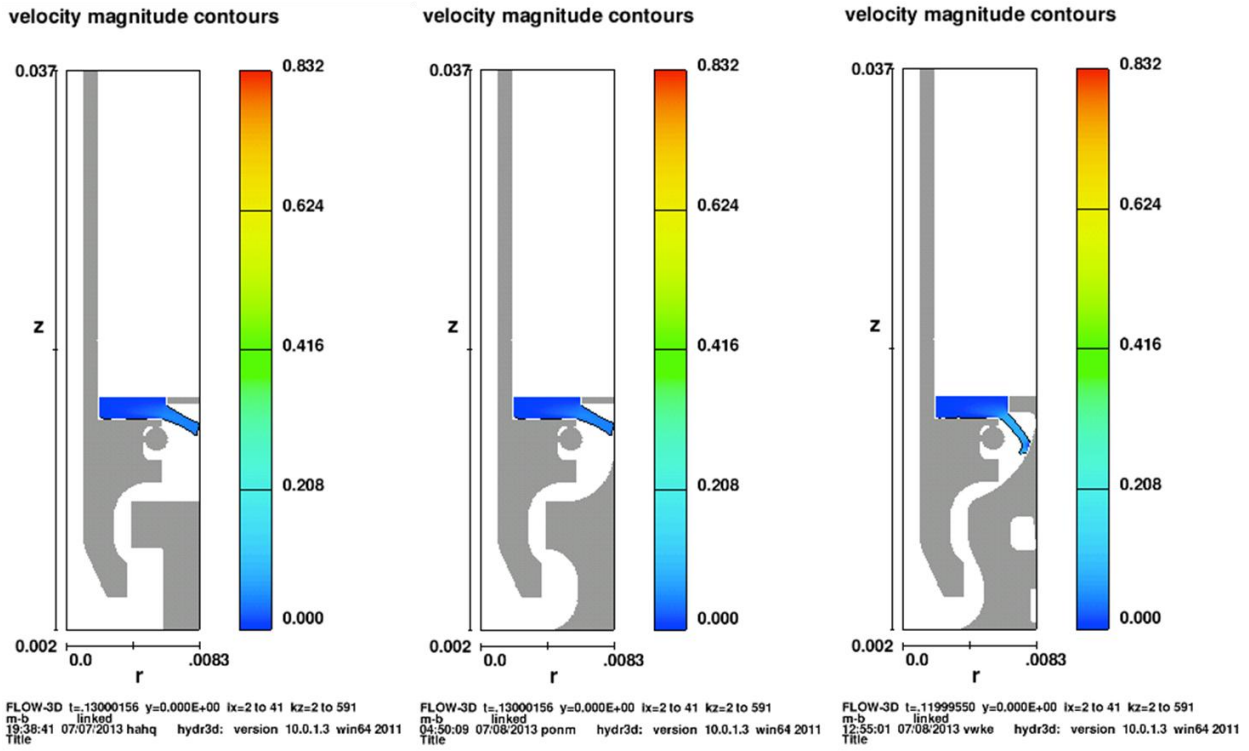
velocity magnitude contours
0.037
0.832
0.624
z
0.416
0.208
0.000
0.002
0.0
.0083
r
FLOW-3D t=.13000156 y=0.000E+00 ix=2 to 41 kz=2 to 591
m-b linked
19:38:41 07/07/2013 hahq hydr3d: version 10.0.1.3 win64 2011
Title
velocity magnitude contours
FLOW-3D t=.13000156 y=0.000E+00 ix=2 to 41 kz=2 to 591
m-b linked
04:50:09 07/08/2013 ponm hydr3d: version 10.0.1.3 win64 2011
Title
velocity magnitude contours
FLOW-3D t=.11999550 y=0.000E+00 ix=2 to 41 kz=2 to 591
m-b linked
12:55:01 07/08/2013 vwke hydr3d: version 10.0.1.3 win64 2011
Title

B.

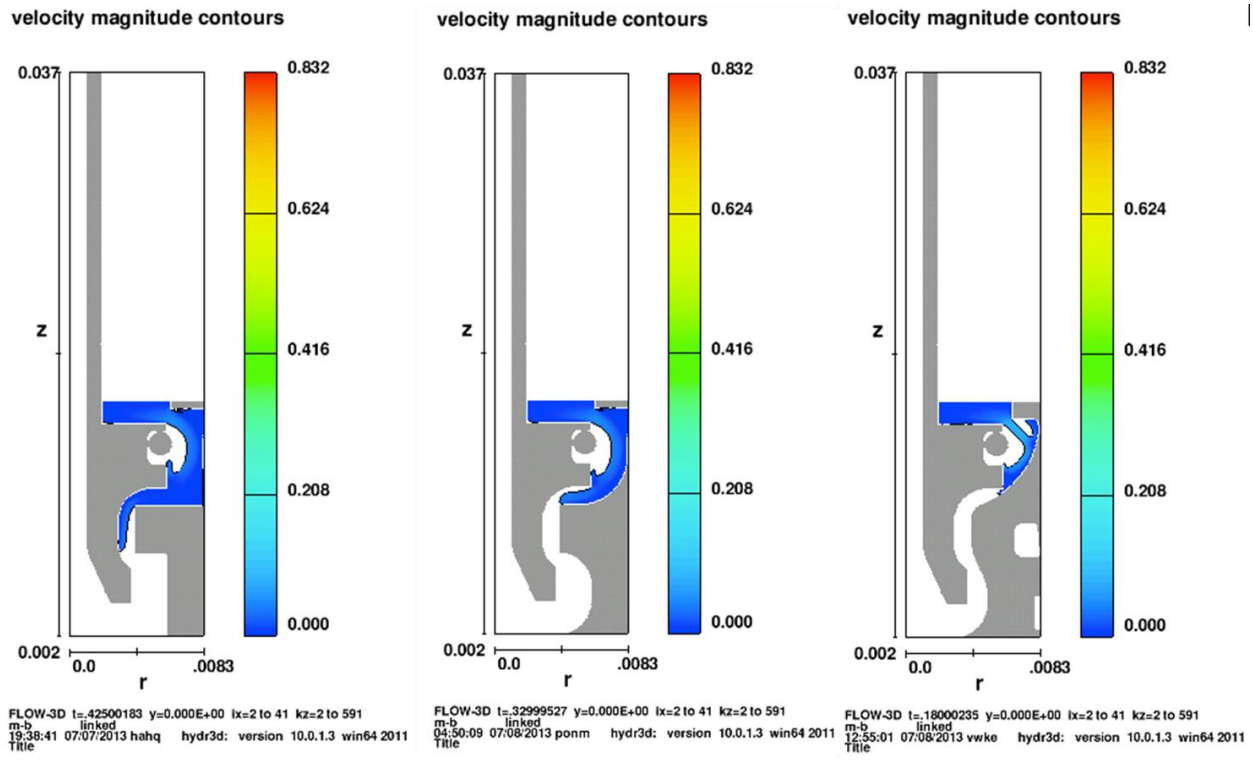
velocity magnitude contours
0.037
0.832
0.624
z
0.416
0.208
0.000
0.002
0.0
.0083
r
FLOW-3D t=.42500183 y=0.000E+00 ix=2 to 41 kz=2 to 591
m-b linked
19:38:41 07/07/2013 hahq hydr3d: version 10.0.1.3 win64 2011
Title
velocity magnitude contours
FLOW-3D t=.32999527 y=0.000E+00 ix=2 to 41 kz=2 to 591
m-b linked
04:50:09 07/08/2013 ponm hydr3d: version 10.0.1.3 win64 2011
Title
velocity magnitude contours
FLOW-3D t=.18000235 y=0.000E+00 ix=2 to 41 kz=2 to 591
m-b linked
12:55:01 07/08/2013 vwke hydr3d: version 10.0.1.3 win64 2011
Title

C.

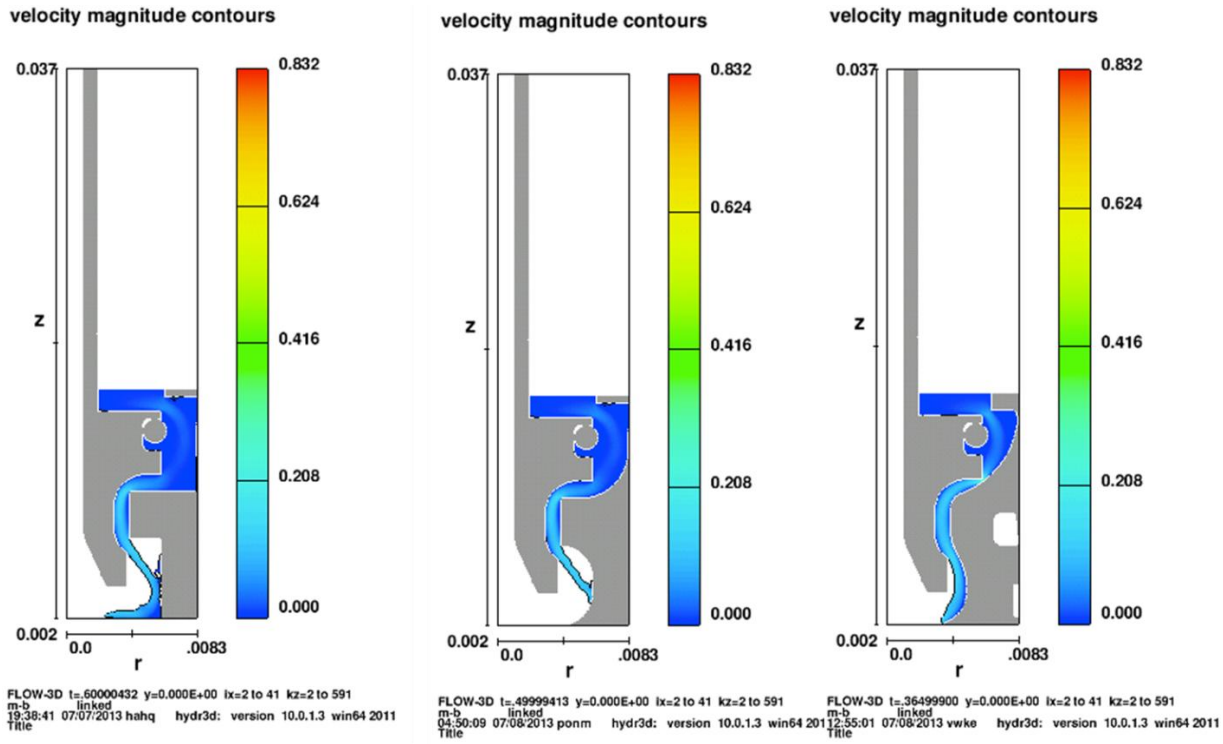

Figure 8: Velocity of jet streams of RRP flow throughout successive designs investigated using CFD models. A. The initial jet velocity became further directed, while the drug chamber was redesigned around the initial water impact within the chamber to increase mixing. B. The shape of the drug chamber was simultaneously reduced and reshaped to allow for great drug mixing and exhaust. C. The secondary chamber allowed further advection of drug within the fluid while directing the solution into the central output shaft.

A.

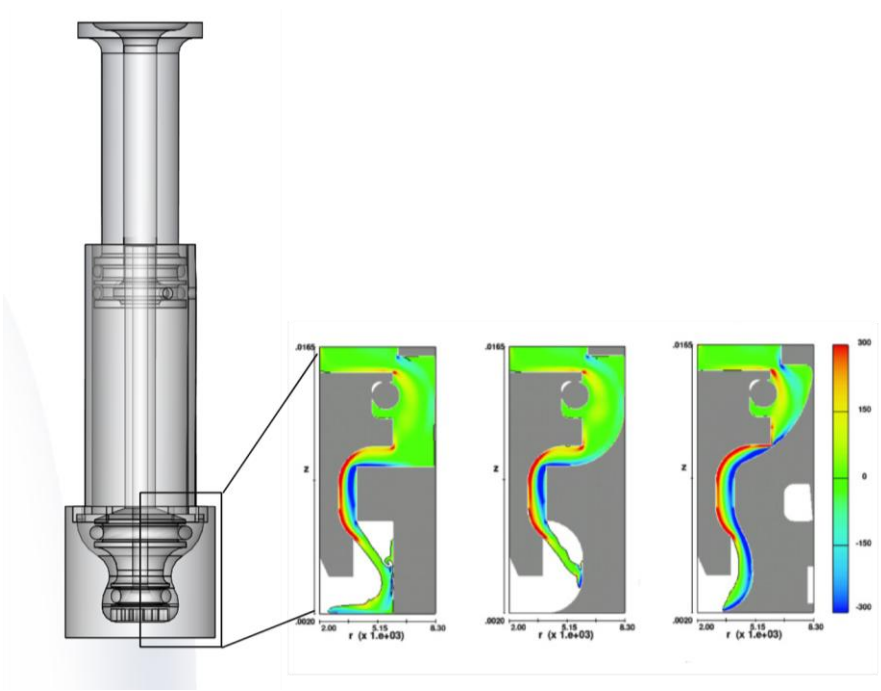

B.

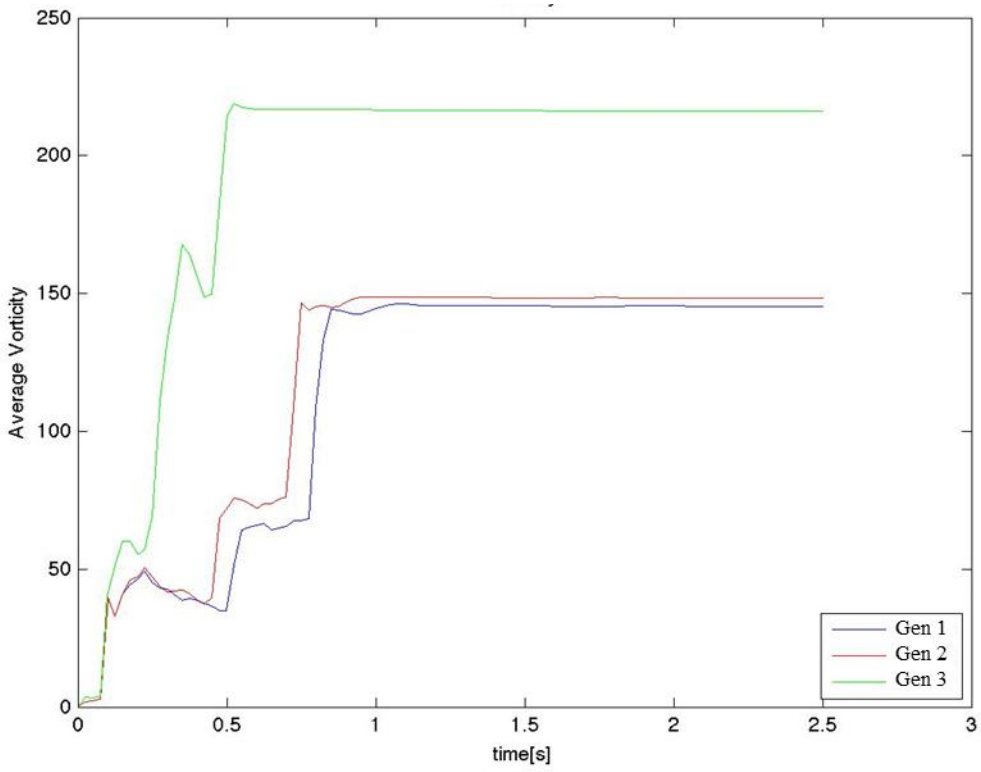

Figure 9: Vorticity simulations. Each subsequent generation of the RRP added more vorticity than the previous, reflecting improvements made with each design. A. Snapshots from simulations of different RRP generations focused on vorticity. B. Average vorticity as a function of time over a 2 second inject for different generations of the RRP used as one of the metrics to measure RRP efficacy.

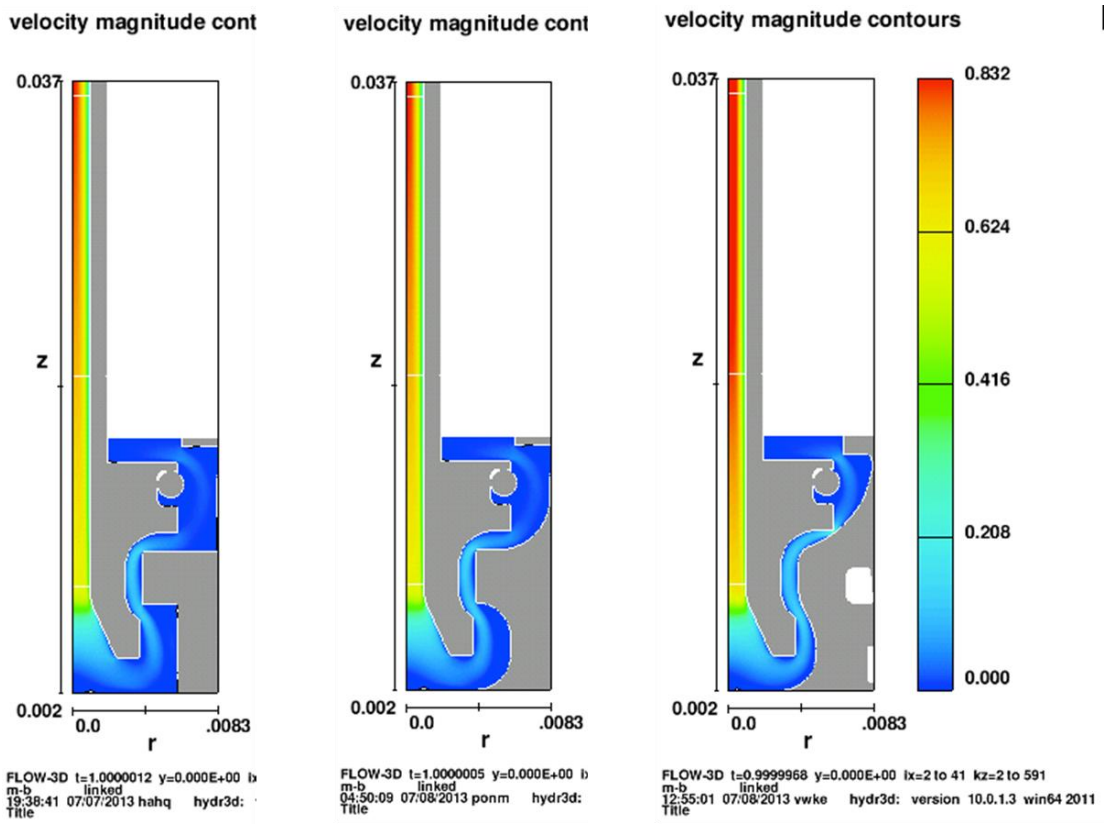

Figure 10: Images from simulation results of the drug mass at the final output through successive generations of RRPs (From left to right: Generation 2, Generation 5, and Generation 7).

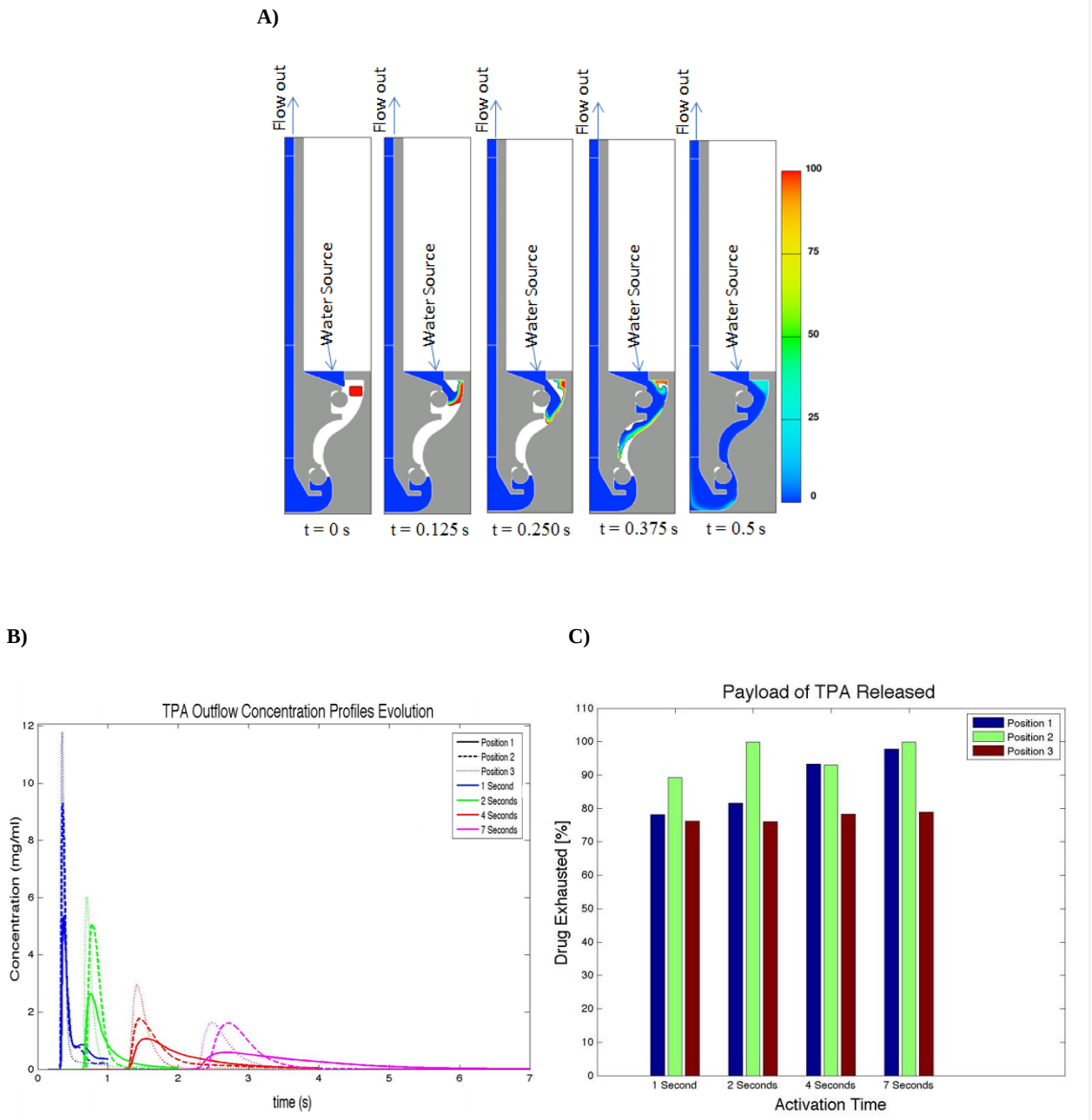

Figure 11: Simulation results from numerical models done in Flow3D. A) Snapshots of the CFD simulation for a 0.5 s injection period. Each frame represents 0.125 seconds of progression. The color gradient indicates the concentration of drug, with dark blue being only water. White background is empty space (modeled as a vacuum). Flow of water in and flow out of elute are indicated on the diagram. B) Simulated outflow concentration profiles at three different positions over four activation times (1 s, 2 s, 4 s, 7 s). Positions depicted are related to the discrete positions represented in Figure 2. C) Percentage of tPA released, or delivered "payload", over the simulated activation times.

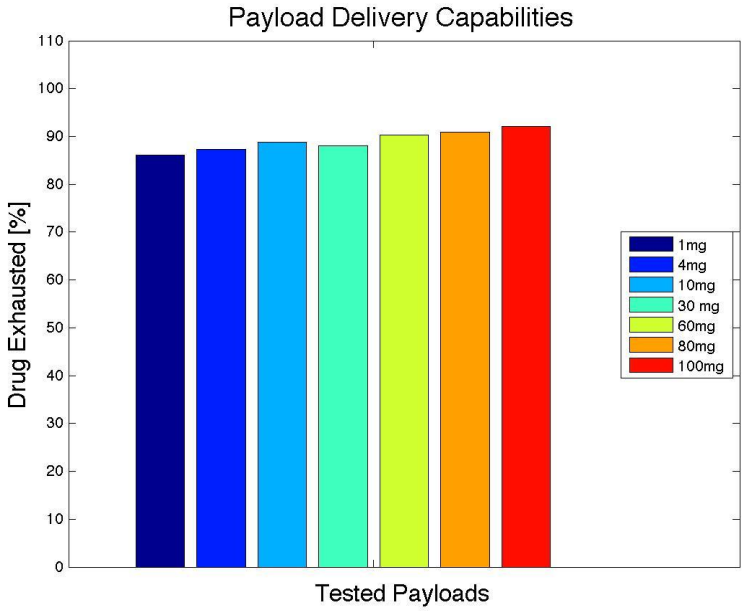

Figure 12: Percentage of payload delivered of different payload masses (1, 4, 10, 30, 60, 80, 100 mg) done in Flow3D. Drug exhausted % was the amount of the modeled drug measured outside the RRP after simulations over the total initial drug modeled.

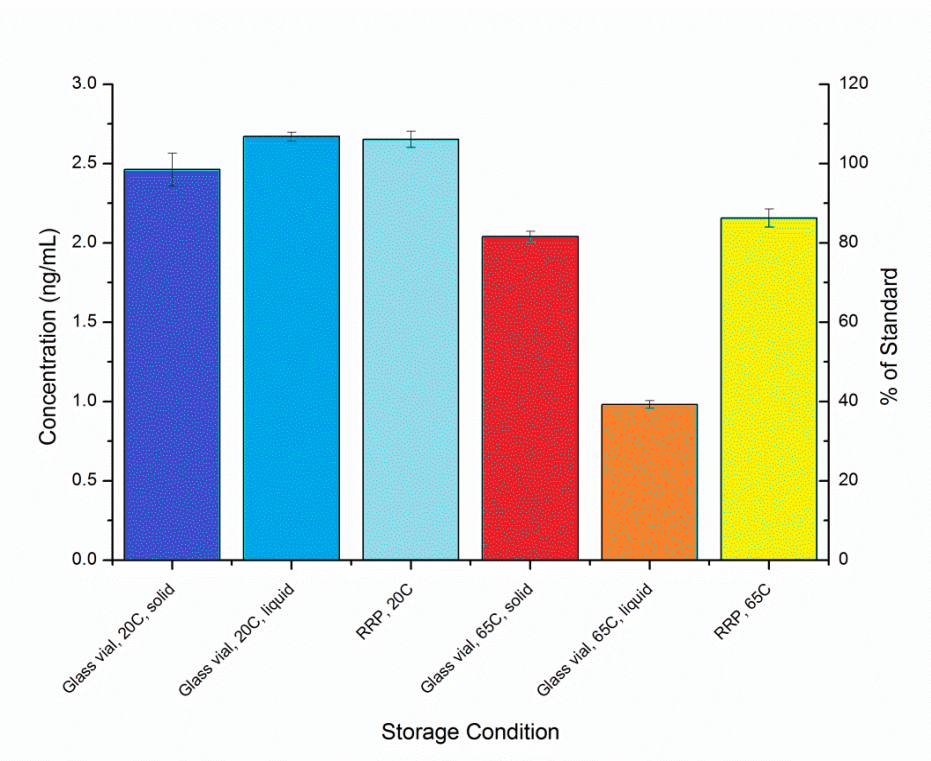

Figure 13: ELISA stability characterization, N = 6 trials. ELISAs were carried out according to standard procedure of the eBioscience Platinum Sandwich ELISA kit for human tPA. Data was read on a Biotek microplate spectrophotometer at wavelength = 450 nm.

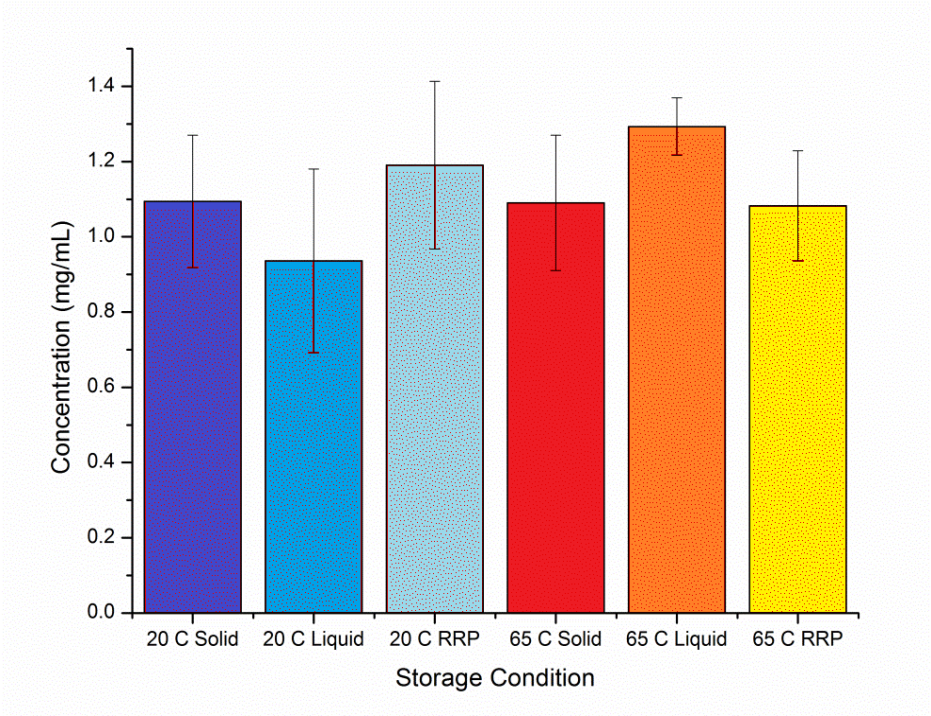

Figure 14: HPLC concentrations of tPA in samples, N = 6 trials. HPLC was carried out on a reversed-phase ZORBAX SB-CN column over a water:ACN:TFA gradient. UV spectrometry to detect tPA was read at 280 nm; fluorescence was read at 275 nm excitation and 340 nm emission.

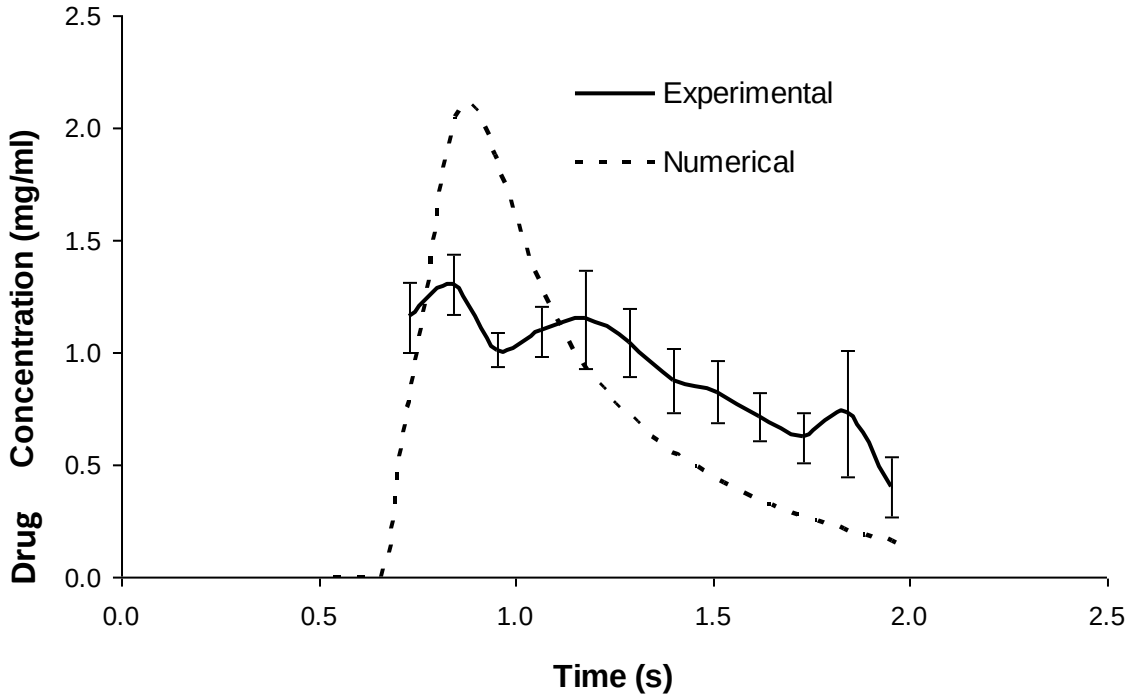

Figure 15: Output concentration profile of the RRP compared to numerical results. N = 8 trials. Data was gathered using a syringe pump set at 259 ml/min flow rate (to match a 2 s inject through a 20 cc syringe). Elute was collected in discretized wells along a tray linearly actuated normal to the syringe outflow. As the linear actuator had constant velocity and was matched with the activation time of the syringe, each sample bin represented 140 ms of flow. Samples were then analyzed through UV-Vis spectrophotometer and plotted relative to time.